Establishing Low-Energy Sequential Decomposition Pathways of Leucine Enkephalin and Its N- and C-Terminus Fragments Using Multiple-Resonance CID in Quadrupolar Ion Guide

V. Sergey Rakov, Oleg V. Borisov and Craig M. Whitehouse

Analytica of Branford, Branford, Connecticut, USA

The simultaneous resonant low-energy excitation of leucine enkephalin and its fragment ions was demonstrated in a collision cell of the multipole-quadrupole time-of-flight instrument. Using low-amplitude multiple-resonance excitation CID, we were able to show the exclusive sequential fragmentation of N- and C-terminus fragments all the way to the final fragments—immonium ions of phenylalanine or tyrosine. In this CID mode the single-channel dissociation of each new generation of fragments followed the lowest energy decomposition pathways observable on the time scale of our experiment. Up to six generations of sequential dissociation were carried out in multiple-resonance CID experiments. The direct qualitative comparison of fragmentation of axial-acceleration versus resonant (radial) CID was performed in the same instrument. In both activation methods, fragmentation patterns suggested complex decomposition mechanisms attributable to dynamic competition between sequential and parallel dissociation channels. (J Am Soc Mass Spectrom 2004, 15, 1794–1809) © 2004 American Society for Mass Spectrometry

Resonant harmonic excitation of ions is the primary method for MS detection and activation of induced dissociation in most ion traps. Simultaneous excitation of ions of different *m/z* ratios is routinely employed to illuminate dissociation pathways using ion traps. It can also be used in harmonic ion guides in order to selectively eject or dissociate ions on their way to an MS analyzer. This paper reports results of validation of a nontrapping multiple frequency component low-energy resonant collision-induced dissociation (CID) in a linear quadrupole ion guide.

Several of the ion activation methods used in modern MS instruments are selective, by nature, and target exclusively the parent ion, supplying no additional energy to its primary fragments. As examples of such methods, the sustained off-resonance irradiation (SORI) [1], or on-resonance CID in ion cyclotron resonance (ICR) cells [2] can be mentioned. Other activation methods, such as infrared multi-photon dissociation (IRMPD), and its variations [3, 4], or black body infrared dissociation (BIRD) [5] are nonselective, by nature, and always excite primary fragments along with the parent ion. A vast majority of ion activation methods may excite primary fragments depending on the condition of the experiment. In such methods, modeling of the dissociation process can be quite complex. For example, in surface induced dissociation (SID) experiments with moderate impact energies, the dissociation event most likely comprises activation of only the parent ion at the surface, followed by its recoil and subsequent unimolecular decomposition. In contrast, at high impact energies, more extensive fragmentation can be observed due to on-surface shattering of the precursor and possibly some of its primary fragments [6].

Axial CID in ion guides (or in triple-quadrupoles) achieved by accelerating the primary ions into the collision cell operated at an elevated pressure is a potentially nonselective activation technique. If initial collisions of the projectile ion with the background gas are sufficiently rapid and energetic, internal energy of the projective ions is increased rapidly to the level, substantially exceeding the dissociation threshold for the dissociation. In such case, the projectile ions dissociate rapidly in the region of nonzero axial potential gradient, and their fragments can be further accelerated. This may lead to energetic collisions of these primary fragments with the background gas, resulting in secondary (sequential) CID.

Resonant activation of ions in harmonic ion guides and ion traps arguably provides a better-controlled

Published online October 28, 2004

Address reprint requests to Dr. V. S. Rakov, Analytica of Branford, 29 Business Park Drive, Branford, CT 06405, USA. E-mail: rakov@aob.com

1044-0305/04/$30.00
doi:10.1016/j.jasms.2004.06.020

Received March 19, 2004
Revised June 24, 2004
Accepted June 24, 2004

experimental setup for CID, compared with axial acceleration. In low-energy resonant CID experiments, primary fragment ions are assumed to fall out of resonance with the excitation, and rapidly cool through collisions with neutral gas, potentially qualifying this excitation method as selective. However, at higher excitation amplitudes and high q-values, resonant-CID events which occur away from the center (axis) may form fragments exposed to energetic high-frequency oscillations. Through collisions with the background gas, such primary fragments will be excited rather than cooled and may undergo secondary fragmentation. Finally, even in activation methods in which no excitation of the primary fragments takes place, internal energy partitioning during primary CID event can cause them to be produced "hot" enough to undergo sequential secondary dissociation.

Optimization and calibration of a new mode of activation is best performed using relatively simple ionic systems for which kinetics and dynamics of gas-phase decomposition has been studied in the past. Many small-to-medium size organic molecules and small peptides possess well-known fragmentation mechanisms and can be used as "gauges" assisting in characterization of new modes and methods of internal ion activation. We intentionally avoid using the term "thermometer ion" for Leucine-enkephalin throughout this work because, for some excitation methods, its dissociation can be slower than activation, (i.e., the observable is slower than the action). In this study, leucine enkephalin was used for evaluation of performance of the multiple-resonance CID experiments. Primary decomposition of this ion has been characterized in a number of kinetic and dynamic studies [7–10] and used - in direct or comparative manner - to estimate the internal energy up-take for a variety of induced-dissociation experimental protocols [11–17]. Overall, its CID spectral patterns have been recorded for a wide range of internal energies using a variety of activation methods.

However, due to dynamic competition between direct and sequential fragmentation channels activated in parallel by most CID techniques, it is hard to assign exact reactions contributing to their CID patterns—even for relatively well studied ions like leucine enkephalin. The b_4 is the primary low-energy fragment of leucine enkephalin. Sequential formation of the a_4 ions from b_4 fragments of leucine enkephalin was established [7], but a direct decomposition of leucine enkephalin ion into the a_4 was also observed [18]. At higher activation levels, the dynamic competition between N- and C-terminus fragments becomes pronounced. Leucine enkephalin (YGGFL) has tyrosine on the N-terminus side, and phenylalanine close to the C-terminus side, providing the possibility of the b-y fragmentation competition—in accord with the common understanding of the roles of the proton affinity (PA) and the mobile proton model [19–22]—in the dissociation process. For smaller parent ions, formation of complementary b- and y-fragments via the so-called b-y pathway has been accurately modeled and was shown to likely follow the proton-bound dimer (PBD) transition state [23–25]. In some cases, relative yield of y- and b- ions was found related to the PAs of dissociation counterparts [26, 27]. Interestingly, in early experimental reports on YGGFL dissociation, relative intensities of "complementary" y_2 and b_3 fragments were found to be indicative of the amount of internal energy deposited into the leucine-enkephalin parent ion [8, 11]. If the PBD transition was the only contributing channel for these ions, and the proton migration on to one of the dissociation counterparts happened (fast) at the final stage of decomposition, such energy dependence would be hard to explain. Another pair of fragments whose relative intensity was proposed as the precursor's internal energy measure is b_4 and a_4. These two ions participate in a sequential dissociation channel $P \rightarrow b_4 \rightarrow a_4$ which is dominant for low-energy excitation, on a millisecond time scale. Therefore, even when no direct excitation of the intermediate b_4 ions takes place, a_4 ions may be formed via secondary decomposition of "hot" b_4 (internal energy partitioning). In slow-activation CID methods this almost never happens because such a process would require high excitation of the precursor ion and a low rate of cooling of the intermediate. But under the conditions of fast excitation, direct channel $P \rightarrow a_4$ becomes accessible.

Spectral patterns of the single-resonance CID of leucine enkephalin in a linear quadrupole ion guide are presented and qualitatively compared with those obtained using axial CID under similar conditions. In both of these activation methods, dependence of the spectral patterns on the activation conditions advocates complexity of the fragmentation mechanism(s). Problems associated with correlating the precursor's energy with relative ion abundances are addressed in the first section of the Results. This section also critically revisits the traditional understanding of the resonant activation mechanism. Overall, the results of the current study indicate a qualitative rather than quantitative correlation between the precursor's energy and relative abundance of b_4 and a_4, as well as y_2 and b_3.

In order to provide additional insights into the possible CID mechanism(s), this study addressed sequential low-energy decomposition pathways of leucine enkephalin and its main fragments. Limited information on these pathways is available. The most extensive study of the leucine enkephalin's sequential decomposition (up to four generations of fragments) was performed in both ion trap and ICR [17] and revealed correlation between the dissociation paths and the time scales of energy uptake and MS detection. It was emphasized that on a ~0.1 ms time-scale of axial CID excitation and detection in a triple quadrupole MS some dissociation channels are not observable due to high activation entropy (although low activation energy). In the resonant CID experiments reported here, estimated transient time of the ions in the collision cell approached 5 ms and a presence of slow rearrangement-

driven decomposition was observed. Dissociation CID channels observed on a millisecond excitation time scale of the presented low-activation multiple-resonant CID experiments corresponded to the lowest-energy channels of sequential gas-phase decomposition. Information on the *sequential* decomposition pathways is critical in understanding the dynamic competition between *parallel* dissociation channels and the mechanism(s) of the formation of complementary ions.

The presented mode of sequential multiple-resonance CID is principally different from the extensive (simultaneous) fragmentation of the moderately-excited parent ion into a broad set of fragments. Not surprisingly, the sets of fragment ions observable by these two CID methods differ. Some of the fragments observed in sequential CID experiments could never be formed in direct CID of leucine enkephalin, and visa versa. Thus, the presented CID mode can be used in tandem with the conventional CID, axial or single-resonance radial, to provide complementary fragmentation information. This makes the low-energy sequential CID a valuable addition to the arsenal of tools—not only for structural studies of the MS^n type or decomposition dynamics investigations—but also for identification of medium-sized unknown peptides based on their dissociation patterns. The MS^6 investigation of leucine-enkephalin emphasizes high parent-to-fragment conversion efficiency, simplicity, and speed characteristic of this method.

Experimental

Instrument Geometry and Operating Conditions

Leucine-enkephalin sample (Sigma, St. Louis, MO) in a 50:50 mixture of methanol:water with 1% acetic acid at a sample concentration of 10 uM was directly injected at a rate of 10 uL/min into a glass capillary electrospray ionization (ESI) source of the new multipole-quadrupole time-of-flight mass spectrometer prototype, described previously [28, 29] and shown schematically in Figure 1. In selected experiments we opted to employ an in-source CID [30, 31] which was realized by creating a high potential gradient in the high pressure region between the capillary exit and the skimmer. Ions sampled by the skimmer continuously entered a 75 mm long ion-collimating hexapole (H1) with an inscribed diameter of 2.75 mm operated at 5.3 MHz radio frequency (RF). The H1 served as a vacuum conductance limit between the two vacuum chambers with estimated pressures of 10 mTorr and low 10^{-5} torr. From the H1, ions were transferred into a 200 mm long, analytical grade quadrupole mass filter (analytical quadrupole, AQ) with 9.25 mm rod diameter and an inscribed diameter of 8.12 mm. The AQ was operated at 1 MHz in a radio frequency-direct current (RF-DC) resolving mode to isolate parent ions or selected fragments of the in-source CID. Pressure in the AQ region was maintained in the low 10^{-5} torr range.

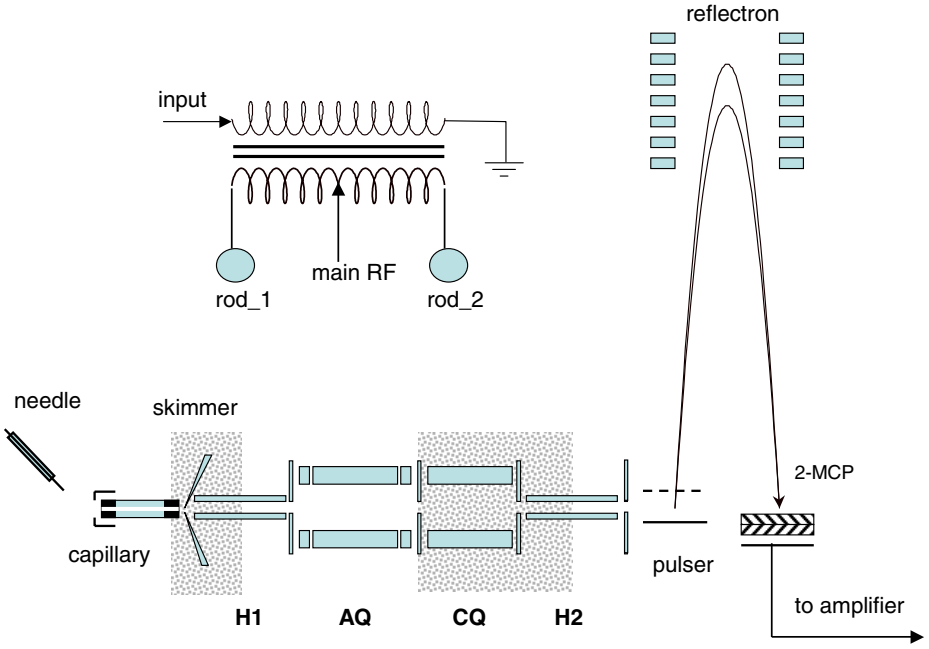

Figure 1. Diagram of the multipole-quadrupole TOF MS instrument. ESI source is equipped with a spray-needle, glass capillary, and a sampling skimmer. The ion guide is equipped with the front hexapole (H1), followed by the analytical quadrupole (AQ), the collision quadrupole (CQ), and the rear hexapole (H2). The CQ and the front part of the H2 reside in the collision cell operated at 10 mTorr pressure of nitrogen. Regions of elevated pressure are indicated by the gray background. The orthogonal TOF MS analyzer features linear single-stage reflectron and an MCP detector. The inset schematically describes the resonant dipolar transformer. The main RF lead supplies one phase of the 1 MHz driving RF; input is provided by the AWG; rod_1 and rod_2 are a pair of opposing rods.

From the AQ, ions were transferred into a collision cell region equipped with another quadrupole (collisional quadrupole, CQ), 120 mm long, with 9.25 mm rod diameter and an inscribed diameter of 8.12 mm, operated in RF-only mode at 1 MHz frequency. In this study, pressure in the CQ region cell was maintained at ~10 mTorr of nitrogen. Axial translation energy of the ions entering the CQ was controlled by a common electrostatic potential offset, superimposed onto individual potentials of all upstream optical elements, from capillary exit to the exit of the AQ. In experiments realizing axial CID in the CQ this common offset was set sufficiently high to accelerate ions selected in the AQ into the CQ and induce dissociation via energetic collisions with the background gas. Alternatively, the axial energy of ions entering the CQ was set low to avoid energetic axial ion-neutral collisions. Instead, activation of ions in the CQ was performed via applying resonant frequency excitation to one rod pair of the CQ, in a dipolar fashion, as described below.

In both of the axial and resonant CID experiments fragment ions were extracted from the CQ in a continuous flow mode without trapping (gating) into a second collimating hexapole, H2, identical to H1. The front of the H2 extended into the collision chamber of the CQ and its rods served as a vacuum conductance limit between the collision chamber and the next vacuum chamber in which the pressure was maintained at a low 10^{-5} torr. In Figure 1 gray color background in the skimmer-H1 and CQ-H2 (front) regions indicates regions of the elevated pressure. In all of the experiments described here, axial potential gradient between the CQ and the H2 was set low to avoid secondary axial CID. The main RF amplitudes of the AQ and/or the CQ were varied as described in the Results and Discussion Section, to insure nondiscriminative transmission in the *m/z* range of interest. Hexapoles have a broader and "flatter" transmission than RF-only quadrupoles; in all experiments, both H1 and H2 were driven by 250 $V_{0\text{-}p}$ RF, providing nondiscriminating transmission over the whole mass range of interest. From H2, ions were continuously extracted into a pulsing chamber of an orthogonal time-of-flight unit maintained at 7.5×10^{-8} torr. The time-of-flight analyzer with linear reflectron and an MCP detector followed by a preamplifier and an analog-to-digital converter-adder was used for the final mass analysis. The TOF-MS data was collected and monitored using Analytica Aviator [32] software.

Resonant Excitation Waveforms and Circuitry

In a linear quadrupole driven by the main RF with frequency Ω ions with mass M and electrostatic charge z undergo radial oscillations with the fundamental frequency

$$\omega = \frac{\beta}{2}\Omega, \tag{1}$$

where β was calculated from approximate formula [33]:

$$\beta = \sqrt{a - \frac{(a-1)q^2}{2(a-1)^2 - q^2} - \frac{(5a+7)q^4}{32(a-1)^3(a-4)} - \frac{(9a^2+58a+29)q^6}{64(a-1)^5(a-4)(a-9)}}. \tag{2}$$

Stability parameter

$$q = \frac{4zV_{RF}}{M\Omega_{RF}^2 r_0^2}, \tag{3}$$

determines the effective potential radial depth [34, 35] and, consequently, the sharpness of the radial resonance in the vicinity of ω: the higher the q, the narrower the resonance. In all experiments described in this report, the CQ was operated in RF-only mode ($a = 0$). In low-vacuum experiments such as the resonant CID reported here, both amplitude and energy dissipation resonances are significantly broadened [36–38]. Therefore, calculating β using eq 2 rather than a simpler [39], more commonly used approximation $\beta = (a + 0.5q^2)^{0.5}$, does not significantly improve the accuracy of calculating ω for CID experiments at a low q. On the other hand, approximation given by eq 2 becomes critical for the resonant ejection (directly related to radial amplitude resonance) experiments performed at lower pressures [40] and at $q > 0.4$. In some of the experiments reported here selected ions were excited at $q > 0.4$. Therefore, eq 2 was used to calculate β throughout this study. For an ion ensemble passing through the CQ that contained K spectral peaks (components) the waveform for simultaneous resonant excitation of any subset of $N < K$ of these peaks was calculated as

$$v_N(t) = \sum_{n=1}^{N} V_n \sin(\omega_n t) \tag{4}$$

without phase randomization. Excitation frequency components ω_n were calculated using eqs 1–3 for a set of $(m/z)_n$, and the amplitudes of these components V_n were assigned individually. In simpler terms, we summed individual resonant sinusoidal excitation waveforms, each with a preselected amplitude level for all desired *m/z* targets.

MATLAB 6.5 was used to generate a digital waveform consisting of one thousand points, using eq 4 with a time step of 1 microsecond. The resulting dataset corresponded to 1 ms of excitation. This digital waveform was sent to one 12-bit digital-to-analog converter channel of the National Instruments PCI-6713 (Austin, TX) arbitrary waveform generator (AWG) operated at a sampling frequency of 1 MHz. The fact that the sam-

pling frequency of the resonant excitation equaled the main-RF was coincidental. The resonant excitation frequency is always lower than the main RF. It was sampled at 1 MHz/point simply to ensure sufficient number of points per excitation period. The main RF was not synchronized with AWG. AWG was operated in a self-retrigger mode allowing 1 ms excitation waveform to be repeated up to several thousand times. One pair of the opposing CQ rods was decoupled in an RF-sense to allow dipolar superposition of the resonant excitation with the main RF [41, 42] as schematically shown in Figure 1. The periodic waveform from AWG with the maximum amplitude of 10 volts zero-to-peak ($V_{0\text{-}p}$) was supplied to one end of the primary coil of the de-coupling transformer with a gain of one, while the other end of the primary coil was grounded. The center point of the secondary coil of the transformer received the main RF signal of 1 MHz, while the end-points of this coil led to two opposite rods. In this configuration opposing rod_1 and rod_2 carry the main RF in-phase while the superimposed excitation waveform has a 180-degree phase shift between rod_1 and rod_2 with an amplitude equal to that on the primary coil input.

Each excitation waveform was applied to the CQ for several seconds without synchronization with TOF MS detection, which proceeded in parallel, updating the spectrum on the computer screen every second (at the TOF-pulse rate of 10 kHz, with a background summation of 10,000 spectra). Thus, the result of applying an excitation waveform could be observed in several "screen-shots." Multiple values of *m/z* and amplitudes as well as the overall duration of excitation (recalculated into the number of retriggers of AWG) were user-selectable.

The multiple-resonant CID method with spectral subtraction for MS^n studies using triple quadrupoles has been previously reported [43, 44]. In a complex CID spectrum the spectral subtraction reveals a cause and effect relation between the excitation applied to a certain ion and its dissociation. In experiments described in the Results section, the resonant CID amplitude was minimized in an attempt to induce dissociation of the excitation target (ion) predominantly into one fragment. Such mode of CID was conditionally termed *exclusive* "one target-one fragment" dissociation when, in the fragmentation spectrum, one of the fragments was more than five times more intense than any one of the other fragments. Comparison of spectra obtained with and without such low-amplitude excitation was straightforward, and although the spectral subtraction could have been used, in this study it was not employed. Nevertheless, we note that the presented method of CID investigation realizes a special case of the general spectral subtraction MS^n CID method in linear quadrupoles. In this work, this general approach was (1) simplified by finding conditions for exclusive decomposition, (2) extended to higher orders of MS, and (3) complemented using an axial or in-source CID to produce the primary fragments.

Results and Discussion

Single-Frequency Component Resonant (Radial Dipolar) CID of Leucine Enkephalin: Qualitative Comparison with Axial CID in the Same Quadrupole

The multiple 2-D trap quadrupole time-of-flight mass spectrometer schematically shown in Figure 1 allows direct comparison of fragmentation patterns achieved by two modes of CID, which we term throughout this work *axial* and *resonant* (*radial*), respectively. The axial CID mode was realized by creating a steep axial electrostatic potential gradient between the AQ and the CQ in the region of elevated pressure, at the entrance of the collision cell.

The primary ion energy corresponding to the axial velocity component was determined by the offset potential applied to the collimating hexapole H1 relative to that of the collision cell quadrupole CQ. This potential difference, for singly charged ions, can be conditionally called the *axial collision energy* of the axial CID in the CQ, although the real picture is more complex. In the first collision, only a part of the translational energy of the ion is converted into its internal energy. Past this first collision, the parent ion may experience a number of additional lower-energy collisions with neutrals, each of which will further increase its internal energy. If these collisions are energetic and occur rapidly, the parent ions may acquire internal energy which significantly exceeds its dissociation threshold energy. Such "overexcited" ions will dissociate rapidly near the collision cell entrance, and their fragments themselves will be axially accelerated onto the gas molecules, causing secondary dissociation. Moreover, due to internal energy partitioning between the dissociation counterparts, the fragment ion may inherit part of the "overexcited" precursor ion's internal energy, making it even more susceptible to subsequent (secondary) dissociation. Dynamic variables responsible for an axial-CID spectral pattern include the electrostatic potential gradient and the pressure gradient in the collision cell entrance region, as well as the energy dependent dissociation rate constants of the parent ion and its primary fragments. An attempt to narrow down the collision energy distribution in the process of the axial CID presents an instrumental challenge since, in most cases, even determination of the axial pressure gradient is nontrivial. Instead, the axial CID in collision cells equipped with multipole RF guides is commonly used as a simple way to achieve extensive deep (or broad) fragmentation of the parent ion.

Figure 2a shows the CID spectrum of leucine-enkephalin isolated in the AQ and accelerated into the CQ, with a 25-volts offset between collimating hexapole H1 and the CQ. The collision cell pressure was main-

tained at 10-mTorr. The CQ was operated at the main RF amplitude of 200 $V_{0\text{-}p}$ (400 $V_{p\text{-}p}$) corresponding to the q-value of 0.18 for the parent (P) ion at m/z 556 Da, and the q-value of 0.83 for the lightest expected fragment, the immonium ion of phenylalanine (F*) at m/z 120 Da. In the Results section, we used m/z, and HZ for frequency, while in the Experimental for m/z, and Hz for frequency, while in the Experimental section m/z notation in eq 3 assumed SI units and ω was the angular frequency in *rad/s*. In the resulting CID spectrum, both N- and C-terminus fragments are present along with internal fragments, including the ion of m/z 205 resulting from formation of y_3 and its further dissociation into its own b_2, termed y_3b_4 in accord with prior-established nomenclature [45–47], and immonium ion of phenyl-alanine with m/z 120. Selected ion intensities as functions of collision energy can be combined into a CID fragmentogram shown in Figure 2b. Intensity of the parent ion in the LAB frame collision energy region between 0 and 25 eV experiences a monotonous decline from about 4.5×10^6 down to 2.5×10^6. The corresponding part of the curve is not shown in Figure 2b. Overall, the fragmentation appears complex and provides no easy clues about its pathways. Since the translational (axial) energy of the incoming parent ion is changed as indicated by the x-axis, one may expect not only (slight) change in the projectile-ion transmission efficiency, but also radial scattering of the activated precursor and its fragments. While dissociation trends depicted by Figure 2b appear very complex, realization of the axial CID itself in our instrumental setup is very straightforward and efficient.

When conducting resonant (radial) CID experiments, the primary ion beam energy was lowered to avoid axial collisional activation. Pressure and the main-RF amplitude in the CQ were unchanged from the axial-CID experiment. The corresponding value of $q = 0.18$ for the parent (P) ion's m/z of 556 was used to calculate the resonant frequency. The resonant excitation sinusoidal waveform was applied to one rod pair of the QC in a dipolar fashion as described in the Experimental Section, formally using $N = 1$ in eq 4. The ions experienced excitation during their single pass though the QC without trapping. The amplitude V_1 of the resonant sinusoid was varied between 0 and 1.5 $V_{0\text{-}p}$ (0 to 3 $V_{p\text{-}p}$), and the resonant (radial dipolar) CID fragmentogram of leucine-enkephalin, shown in Figure 3, was obtained. Both Figures 2 and 3 are experimental fragmentograms rather than breakdown curves, in a sense that their x-axes represent experimental conditions responsible for excitation, rather than an internal energy of the precursor ion.

Most abundant fragments observed in the resonant CID were the same as in the axial CID, while their relative abundances as well as their dependence on the control parameters were very different. The latter fact was not surprising, taking into account the difference in activation protocols realized by these two methods. In an ideal case of resonant CID, activation of the precursor ion is selective, providing no additional excitation to its direct primary fragments. Contrarily, these newly-formed fragments must be greatly out-of-resonance with the applied resonant excitation of the parent ion, and should therefore undergo collisional cooling in both internal and translational energy senses. In reality, in both axial and radial (resonant) CID excitation of primary fragments may occur, as explained above. In the axial CID the mechanism for such excitation resides in the axial acceleration of primary fragments and in the primary CID energy partitioning. In the resonant CID, secondary excitation may occur due to the fast oscillations of primary fragments at a high q and radii (causing collisions with gas molecules). On the other hand, when the q-value is low (the effective potential

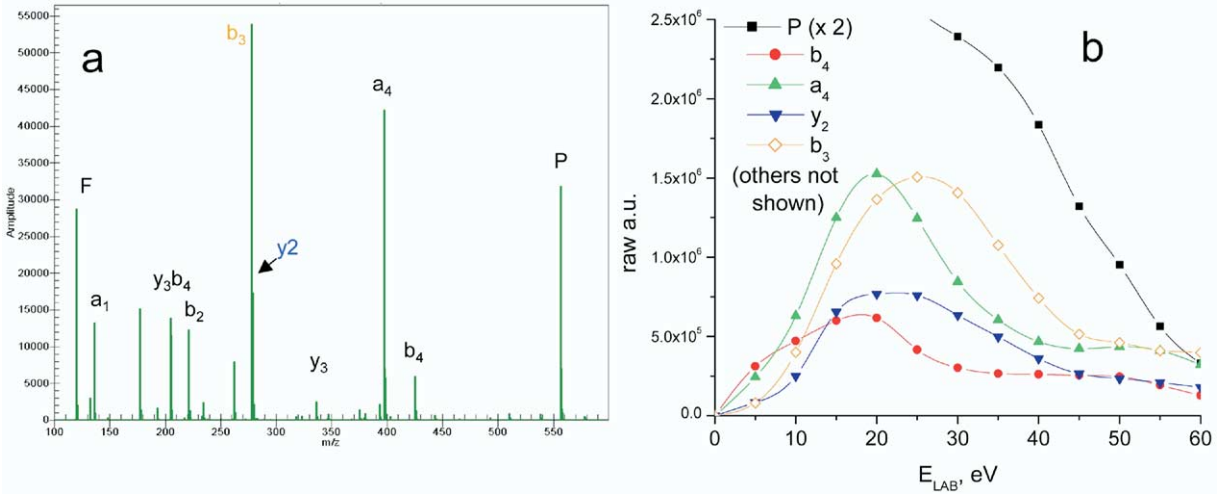

Figure 2. Axial acceleration CID of leucine enkephalin. (**a**) Typical spectrum of YGGFL undergoing a 25 eV (LAB-frame) CID in the CQ region operated at 10 mTorr pressure of nitrogen; main RF amplitude levels and axial potential gradient profile are described in the text; (**b**) fragmentogram of YGGFL versus CID energy (LAB-frame).

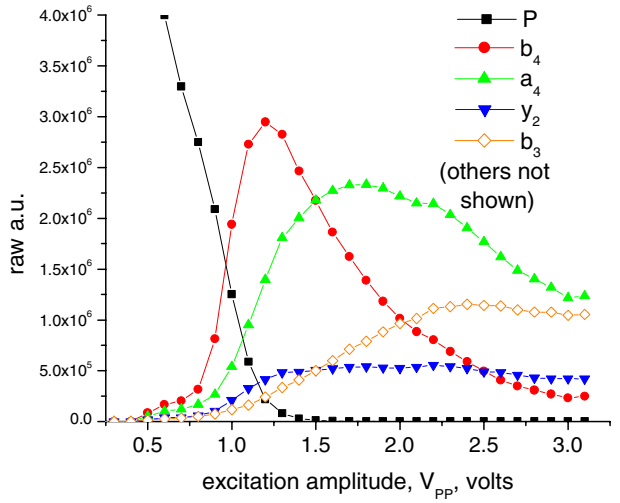

Figure 3. Fragmentogram of YGGFL undergoing single-frequency resonant dipolar CID in CQ versus excitation amplitude; pressure and main RF level conditions are unchanged from experiments of Figure 2.

well is "shallow") and the pressure is high, the ion resonance broadens. Under these conditions, the resonance targeting the parent ion may extend its shoulder to primary fragment(s) of close *m/z*. While curves shown in Figure 3 may appear simpler and "cleaner" compared with those in Figure 2b, the derivation of an exact mechanism of dissociation is not straightforward.

The qualitative inspection of the behavior of N-terminus fragments' curves in Figure 3 reveals interesting trends. It appears that the sequential decomposition $P \rightarrow b_4 \rightarrow a_4 \rightarrow b_3$ might occur, while the y_2 fragmentation pathway seems to stand separately. From the previous studies the b_4 is known to be the primary fragment of leucine-enkephalin, and the a_4 curve suggests that it might have been produced in a secondary fragmentation reaction from b_4. In turn, the b_3 curve could indicate its production from a_4. The internal energy partitioning as the mechanism for secondary activation must be ruled out. Under conditions of slow, multiple-collision activation of the parent ion, the internal energy uptake process must be slower than dissociation. In such a process, the internal energy distribution of the parent ion ensemble is constantly being depleted, from above, by its decomposition. It is unlikely that primary fragments of such a process are "hot" enough to undergo sequential decomposition. Therefore, a low-q/high pressure broadening of resonance, and/or a high-q/high radius fast oscillation motion of primary fragments remain as a possible cause(s) for secondary activation of N-terminus fragments.

On the other hand, b_4 is probably not the only allowed "transition" from the parent ion to a_4, and neither is a_4 the only possible precursor for b_3. In fact, direct formation of a_4 from P has been documented in the past [18]. Transition states leading to direct dissociation of the parent ion into a_4 and b_3 may require high internal activation of the parent ion which, in fact, becomes available at high excitation amplitudes. As a result, direct dissociation channels such as $P \rightarrow a_4$ and $P \rightarrow b_3$ may be activated in parallel with the lower-energy $P \rightarrow b_4$. Once the activation energy for such a channel is exceeded, the reaction rate is determined by both the internal energy and the activation entropy. Thus, energetically expensive dissociation channels may, in principle, become dominant when the parent ion is overexcited due to low cost in entropy [48]. For example, if they require less structural rearrangement of the parent on its way along the reaction coordinate to the transition state or even on the way from the transition state to the products. If b_4, a_4, and b_3 were produced in parallel competing reactions directly from the parent ion, it is plausible that at a high activation level, the rate of $P \rightarrow b_3$ was higher than that of $P \rightarrow a_4$, and higher than $P \rightarrow b_4$. Then, the correlation in relative abundances of b_4, a_4, and b_3 could be a result of entropy driven competition between *parallel* channels.

Relative abundance of complementary b_3 and y_2 fragments has been noticed as indicative of the amount of the internal energy deposited into the parent ion [8, 11]. Formation of y_2 was referred to as the "cold channel" while that of b_3 was termed "hot". Figure 3 may suggest that formation of y_2 is induced at a lower excitation amplitude than b_3, thus confirming that y_2 is lower-energy product of the G-F amide bond cleavage than b_3. That would be true if both y_2 and b_3 had originated from the parent ion directly via the same transition state, (e.g., a PDB which was accurately modeled in the past for smaller amino-acids [23–25]). However, energy dependence of the relative intensities of b_3 and y_2 do not provide direct evidence of this mechanism. Namely, the weak energy dependence of the y_2 curve compared to the strongly featured b_3 may suggest that a set of dissociation channels contributing to formation (and possibly depletion) of these two ions may be unrelated. In order to obtain additional information on the possible origins of the main leucine enkephalin fragments and their own decomposition products, the multiple-resonant experiments presented below were staged.

Multiple Frequency Resonant Low-Energy Sequential Decomposition of Protonated Leucine-Enkephalin: N-Terminus Fragmentation Pathway

The next series of experiments shown in Figure 4 was realized sequentially at a low-level activation of leucine enkephalin fragment ions at the main RF level of 280 $V_{0\text{-}p}$ driving the CQ and the pressure of 10 mTorr in the collision cell. It was performed in sequential excitation stages of a continuous beam of ions passing through the CQ. In the first stage resonant excitation was applied only to the parent ion at variable amplitude. Based on the fragmentation observed, the amplitude of excitation

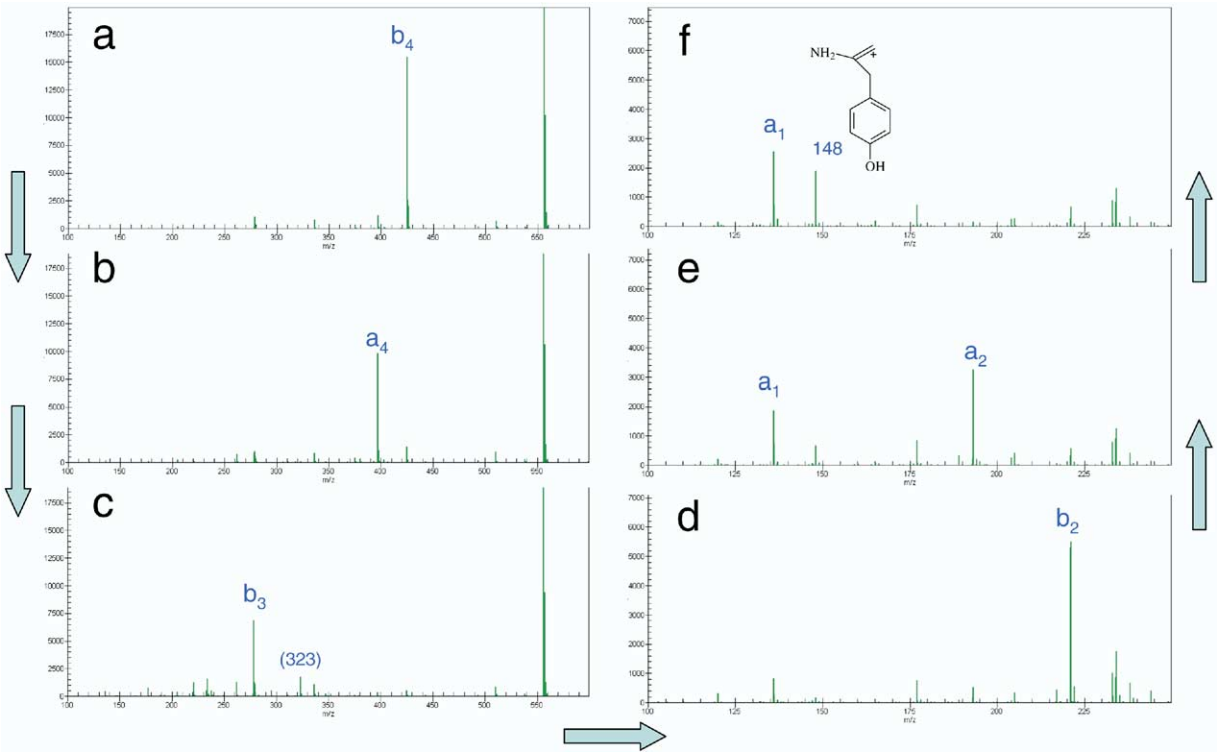

Figure 4. Multiple-resonance CID of the N-terminus of YGGFL. Amplitude levels, CID targets, *m/z* and *q*-values, and resonant frequencies are summarized in Table 1. (**a**) excitation applied only to the parent ion P; (**b**) excitation applied to P and b_4; (**c**) excitation applied to P, b_4, and a_4; (**d**) excitation applied to P, b_4, a_4, and b_3; (**e**) excitation applied to P, b_4, a_4, b_3, and b_2; (**f**) excitation applied to P, b_4, a_4, b_3, b_2, and a_2. For discussion of the sequential fragments, see text.

was adjusted in iterative fashion to achieve exclusive fragmentation of the parent into only one fragment—the b_4 ion. In the next step, an additional frequency component resonant for the b_4 ion was added to the excitation waveform. The amplitude of the component responsible for the parent-ion excitation was kept at the level optimized in the previous step, while the amplitude of the b_4 excitation component was varied until only one of its fragments, a_4 was active. Next, a resonance for a_4 was added, and its amplitude was varied to activate only the formation of b_3, etc. Table 1 summarizes amplitude levels, frequencies and target ions. It also references stability *q*-parameter for all *m/z* values.

The series of spectra referenced in Table 1 were combined into Figure 4, which presents the step-wise sequential decomposition CID of the N-terminus. In Figure 4, the y-axis units are of the raw intensity and are consistent. The y-scale is from 0 to 18,000 in Figure 4a through c, and from 0 to 7500 in Figure 4d through f. The mass scale is 0 to 600 Da in Figure 4a through c, and 0 to 250 in Figure 4d through f—in order to focus on the low-mass fragments. In most of the steps involved in

Table 1. Multiple resonance waveform definition for the N-terminus fragmentation of YGGFL The first column specifies the number assignment for each excitation component, in the context of eq 4 (i.e., $n = 1, \ldots, N$). Column 2 names the target ion; column 3 lists its *m/z* value, in Da; column 4 shows its resonant frequency calculated using eqs 1–3; column 5 specifies the optimized amplitude level, in volts, 0- P, used in eq 4. Column 6 lists the corresponding the stability parameter q_s (see eq 3). Analytical forms used in a numerical generation of the excitation waveforms are shown in Column 7. The Figure references to the spectra resulting from applying excitation are listed in Column 8.

	. . . adds (new) target						
n	ion	$(m/z)_n$ Da	ω_n kHz	V_n	q_i	Final waveform, $\nu_N(t)$	Fig.4
1	P	556	88.4	0.5	$q_{556} = 0.25$	$\nu_1 = V_1\sin(2\pi\omega_1 t)$	a
2	b_4	425	113.1	0.5	$q_{425} = 0.32$	$\nu_2 = \nu_1 + V_2\sin(2\pi\omega_2 t)$	b
3	a_4	397	123.7	0.5	$q_{397} = 0.35$	$\nu_3 = \nu_2 + V_3\sin(2\pi\omega_3 t)$	c
4	b_3	278	173.2	0.6	$q_{278} = 0.49$	$\nu_4 = \nu_3 + V_4\sin(2\pi\omega_4 t)$	d
5	b_2	221	222.7	0.7	$q_{221} = 0.63$	$\nu_5 = \nu_4 + V_5\sin(2\pi\omega_5 t)$	e
6	a_2	194	254.6	1	$q_{194} = 0.72$	$\nu_6 = \nu_5 + V_6\sin(2\pi\omega_6 t)$	f

this series, decomposition of the CID target was exclusive (i.e., resulted in formation of only one fragment). Under such conditions, direct visual comparison of spectra obtained with and without excitation of this particular target clearly revealed the effect of the excitation. It has to be noted that each one of the Figure 4 spectra is not a true MS^n spectrum, in a sense that the CID targets were not isolated and the spectral subtraction was not used.

Production of the primary b_4 via resonant excitation of the parent ion is shown in Figure 4a. By adding a resonant frequency component for the b_4, to the excitation waveform, the latter ion was fragmented further into a_4 as shown in Figure 4b. the additional low-amplitude excitation of a_4 resulted in spectrum shown in Figure 4c. Here, b_3 was the dominant fragment. However, observation of a minor feature at the *m/z* 323, which was brought to the authors' attention by Professor Glish, was quite remarkable. In the prior low-energy CID experiments using ion traps, observation of this ion led to the discovery of a unique rearrangement-driven mechanism of the fragmentation of a_4 [49]. This dissociation channel, resulting in a loss of internal amino-acid, could be observed only using very long "soft" excitation in the ion traps or ICR, but not in the axial CID using triple quadrupoles, or the sector MS. The rearrangement required to realize this dissociation channel was complex, and while this was found to be, in fact, the lowest-energy dissociation channel for a_4, it was too slow to be detected in the CID using nontrapping instruments. The fact that *m/z* 323 fragment ions were observed in the present nontrapping CID experiments qualifies its excitation protocol as slow and bridges the gap between the excitation dynamics of traps versus nontrapping collision cells.

Formation of the b_3 ions from a_4 is noteworthy from another prospective as well. Relative abundance of complementary b_3 and y_2 ions, in leucine enkephalin CID is often noted as a qualitative measure of the precursor's excitation energy. In principle, these ions could be produced via PBD transition state with the last step of the reaction realizing competition for proton in accord with the b_N-y_M mechanism described in detail by Paizs et al [23–25]. Importantly, formation of b_3 from a_4 depicted in Figure 4c is a principally different reaction in which b_3 is complemented by the immonium ion of phenylalanine, as explored in Section III below. Therefore, b_3 depicted in Figure 4c is formed in a reaction which is different from the direct dissociation of leucine enkephalin into b_3. In Figure 4 series, immonium ion of phenylalanine was unstable due to the low-mass cutoff in CQ; in a separate experiment presented below, similar experiment at lower *q*-value was conducted. As discussed above, it is unlikely that the only pathway from an overexcited leucine enkephalin to its b_3 ion goes through b_4 and a_4 sequential intermediates. Thus, the cumulative activation energy used in three steps of sequential $P \rightarrow b_4 \rightarrow a_4 \rightarrow b_3$ decomposition is not relevant to that of the direct $P \rightarrow b_3$ dissociation. After being excited in turn, the b_3 fragment dissociated readily, and almost exclusively, into b_2, see Figure 4d. Formation of a_3 ion from the b_3 fragment was not observed probably due to a relatively greater stability of b_2 ion with resonance charge delocalization compared to the a_3 ion.

From the next fragmentation step of b_2, decomposition became less exclusive. In Figure 4e, the main feature indicated formation of a_2 from b_2, along with a nonnegligible yield of a_1 ions and the *m/z* of 148. In the next step, a_2 was resonantly excited resulting in an additional production of a_1 and the *m/z* 148 ion, as shown in Figure 4f, suggesting that the *m/z* 148 ion was formed from a_2 via a neutral loss of 45 Da. The structure for the *m/z* 148 ion proposed based on the exact mass assignment within the 5 ppm mass measurement accuracy of our instrument is shown next to its peak in Figure 4f. However, the loss of a 45 Da neutral is not typically observed in peptide fragmentation and probably requires internal rearrangement. To the best of our knowledge, no reports have been published that describe the mechanism of neutral 45 Da loss (possibly the carbon monoxide and ammonia, simultaneously). A detailed investigation of this mechanism is underway. To elucidate the pathway of a sequential CID of b_2, a separate study using a smaller model peptide, YGG, was conducted. It was proposed that the structure and stability of its b_2 fragment duplicates that of the b_2 obtained from b_3 of leucine enkephalin. The YGG CID experiments were performed at a lower *q*-value compared to those shown in Figure 4, thus providing a "softer" excitation. The major primary fragment of the YGG CID was the b_2 fragment. When the low amplitude resonant excitation targeting b_2 was added, the major dissociation channel remained $b_2 \rightarrow a_2$, while the production of the *m/z* 148 ion from b_2 was suppressed. In contrast, the formation of a_1 from b_2, maintained its (minor) presence even at low excitation amplitudes. Similarly, when a_2 (from $YGG \rightarrow b_2 \rightarrow a_2$) was added to the list of targets, it dissociated simultaneously into a_1 and the *m/z* 148 ion.

Two things played against the simultaneous low-level excitation of several generations of fragments. As we progressed along the sequential CID path at a constant main RF amplitude in the CQ, each new step produced lighter fragments, at higher q-values. While the fundamental stability criterion dictates low-mass cutoff at $q > 0.9$, high pressure can "stabilize" ions whose *q*-value is even higher than 1, like in the case of the a_1 ion with *m/z* 136, whose *q*-value was ~1.05. However, the effect of collisional damping was not strong enough here to stabilize phenylalanine immonium ion at *m/z* 120. Separate experiments at lower *q*-value are described below. Regardless of the stability problem, increasing *q*-value corresponds to deeper effective conserving potential (i.e., to a proportionally

higher resonant frequency). At the same time, a collision cross section decreased as newly-formed ions became smaller. Together, the last two factors dictated that ion-neutral collisions occur less frequently, and ions had more time to gain velocity prior to colliding with a neutral. Additionally, for smaller ions, a nitrogen molecule acted as a larger collision agent increasing the center-of-mass energy conversion factor. The net result was that ion-neutral collisions become less frequent but more energetic, and the concept of a slow, incremental internal energy increase failed to be an accurate model for the activation process. Therefore, it became difficult to realize a unique, exclusive fragmentation of ions lighter than b_2, simultaneously, with the heavier fragments. In simple terms, it is easier to study small fragments starting from smaller parent ions at lower *q*-value. Nevertheless, when sequential decomposition of YGG peptide was investigated using a lower *q*-value, fragmentations of b_2 into a_2, and a_2 into a_1 were not exclusive, possibly suggesting that the effective mass of the colliding agent was the dominant factor. In order to resolve this problem, a lighter collision gas could be used.

The second factor to be aware of in the multiple-resonance CID of the ions passing through the CQ without trapping was the limited time available for decomposition. In presented experiments, the overall time that the ions spent traveling through the CQ was few milliseconds. The next stage of ion transport through the collimating hexapole and the TOF-MS detection occurred much faster. The duration of the ions traveling through the CQ limited the time allowed for the overall CID to occur. The sequential dissociation experiments shown above required that the intermediate CID stages were completed within the CQ on a time scale of a single pass. From this point of view, the last generation of CID was probably realized closer to the end of the CQ on a short time scale. In order to observe it we probably overexcited the last stage precursors which could have caused a simultaneous opening of the parallel dissociation channels. In order to remove this constraint, the same experiments could be performed with ion trapping in the CQ.

Overall, the low-excitation sequential fragmentation of leucine-enkaphalin presented two cases of a common $b_n \rightarrow a_n$ reaction [50–52] for n = 4 and n = 2, and a characteristic by-pass of the a_3 fragment (YGG-a) via the direct reaction of $b_3 \rightarrow b_2$. The overall sequential resonant CID experiment suggested that once the leucine was lost from the C-terminus as a neutral (and b_4 was produced), the charge was always retained on the amino-terminus side. This proved the previously suggested oxazolonium structure of b-ions with the charge localized within the oxazolone ring.

Sequential Decomposition of Other Primary Fragments: C-Terminus Fragmentation Pathways

The formation of y-fragments from protonated leucine-enkephalin in a millisecond resonant CID requires more energy than the production of b_4 or a_4. The in-source CID method [30, 31] was employed to generate primary y-fragments. The parent ions exiting the ESI capillary were activated via energetic collisions with background gas in the high-field/high-pressure region in front of the sampling skimmer and transmitted into the collimating hexapole (H1), where most of the dissociation took place. In the following analytical quadrupole (AQ), each of the y-fragments of interest was isolated by the RF-DC selection and transferred into the collisional quadrupole (CQ) with a low axial velocity. In the CQ, each of the y-ions' sequential decomposition was then explored using the multiple resonance CID experiments analogous to those used to study the N-terminus pathway.

The first y-fragment to undergo a sequential CID investigation was y_4. Figure 5a shows an in-source CID spectrum of leucine enkephalin obtained at the ~50 volts/mm field gradient in the 1-torr region between the capillary exit and the skimmer.

The enlarged scale inset focuses on the fragments achieved by this nonselective CID method. The AQ RF amplitude (~495 $V_{0\text{-}p}$) corresponded to the apex of the stability diagram for y_4 (*m/z* 393), and CQ was operated at an RF amplitude of ~175 $V_{0\text{-}p}$ corresponding to the *q*-value of ~0.2 for the y_4. The high *q*-value in AQ, combined with relatively low field in the capillary-skimmer region explains a high abundance of the "left-over" parent ions and the absence of low-mass fragments in the spectrum shown in Figure 5a. In the next step, the y_4 fragments were selectively transmitted through the AQ with approximately a 3-Da-wide *m/z* window, which produced a spectrum shown in Figure 5b. The presence of traces of the lower-mass fragments (identified below) in the spectra was the result of the post-isolation dissociation of y_4 inside the collision cell CQ due to the energy partitioning from the highly excited leucine-enkephalin parent ion.

After addition of resonance for the y_4 ions, the spectrum shown in Figure 5c was obtained. It featured a pronounced formation of the y_4b_4 ions (a loss of neutral leucine from the carboxy-terminus of y_4). Small traces of this ion were originally present even before the y_4 was excited, as shown in Figure 5b. Simultaneously with this major channel, a formation of *m/z* 375 (loss of water from y_4), *m/z* 347 (loss of carbon monoxide and water from y_4), and y_2 was observed, as shown in Figure 5c. When the second frequency component targeting the y_4b_4 ion was added to the excitation waveform, the latter readily dissociated primarily into the immonium ion of phenylalanine F*, with a minor presence of *m/z* 217 formed by a loss of 45 Da from y_4b_4 ion (carbon monoxide and ammonia), as shown in

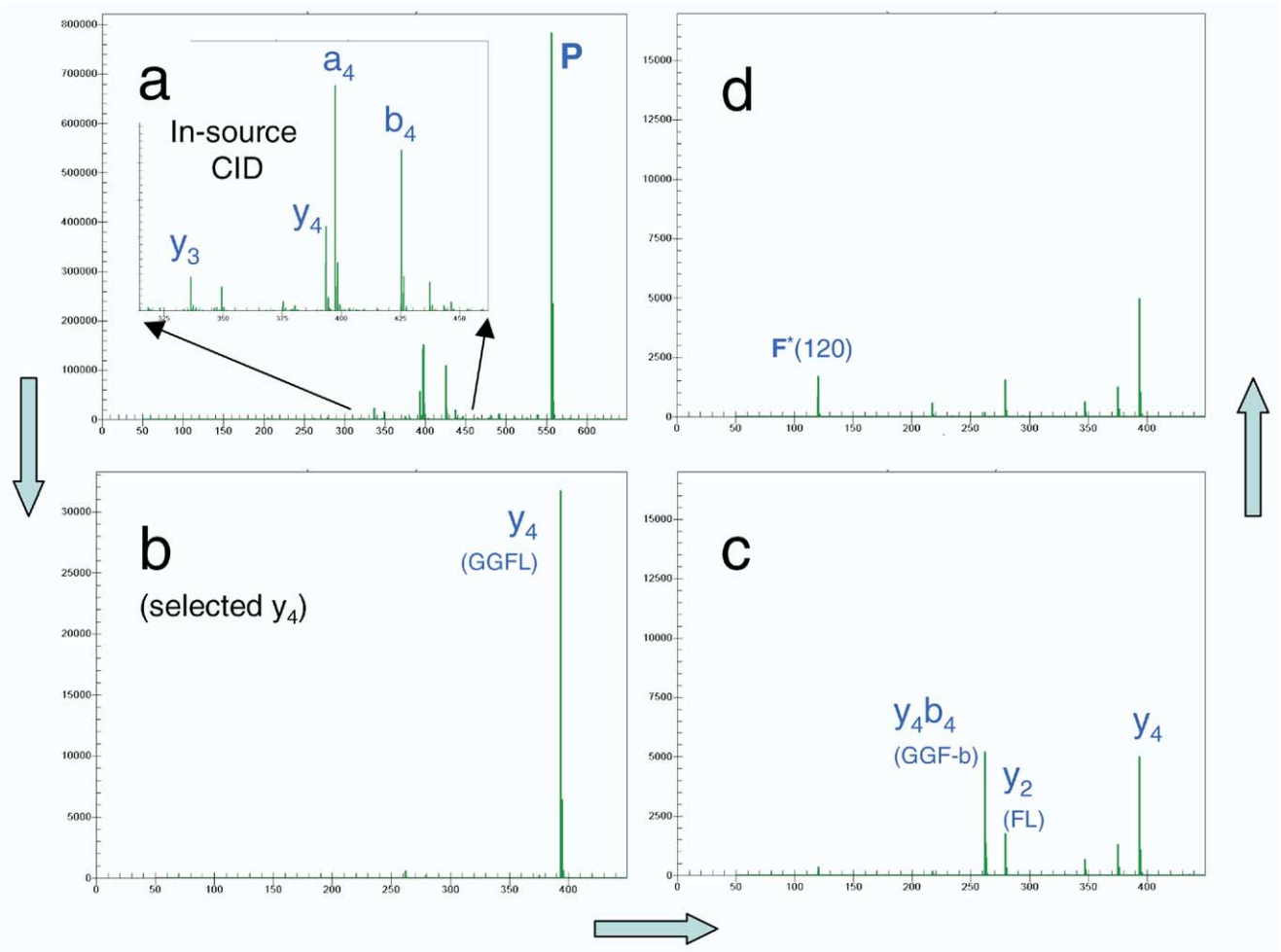

Figure 5. Multiple-resonance CID of the C-terminus fragment y_4 of YGGFL. Main RF levels are described in the text. (**a**) In-source CID spectrum of YGGFL; (**b**) spectrum of the y_4 produced by in-source CID and isolated in AQ; (**c**) resonant excitation applied to the y_4 in CQ; (**d**) excitation applied to y_4 and y_4b_4.

Figure 6d. The dominant dissociation pathway $y_4 \rightarrow y_4b_4 \rightarrow F^*$ suggested that once tyrosine had been lost from the N-terminus of YGGFL, the charge remained localized at the phenylalanine amide nitrogen, and somehow made the F-L region more vulnerable for cleavage than the G-F region. After the backbone was cleaved in the F-L region producing the y_4b_4 fragment (GGF-b), its own weakest point became the G-F region. In the next decomposition step, F* continued to hold the charge, while the GG aggregate broke-off as a neutral. The sequential formation of y_3 from y_4 was not observed, suggesting that the backbone site between the two glycines G-G was a "stronghold", at least while leucine remained on the C-terminus.

In the next experimental series shown in Figure 7, the y_3 (*m/z* 336) fragment of the in-source CID of leucine enkephalin was selectively passed through the AQ with a ~3 Da *m/z* window and subjected to a resonant CID in CQ. Similarly to the case of y_4, the resonant excitation of y_3 in the CQ was performed at a *q*-value of ~0.2 (at main RF amplitude ~150 $V_{0\text{-}p}$). The single-frequency excitation of y_3 produced spectrum shown in Figure 7b, where the major fragment was the y_3b_4 ion at *m/z* of 205, which is the b-ion resulting from the loss of leucine from the C-terminus of y_3 (GF-b). Simultaneously, a low-abundance fragment with *m/z* 177 was identified as the a_2 product of the y_3 itself, termed here y_3a_4 (GF-a). When, in the next step, excitation of the y_3b_4 ions was added, it became apparent that y_3a_4 was a product of y_3b_4, as shown in Figure 7c. Finally, when the y_3a_4 was resonantly excited, it produced one major fragment—immonium ion F* at *m/z* 120. The $y_3b_4 \rightarrow y_3a_4$ step was not surprising, since the structure for its precursor was probably not different from a typical four-amino-acid b-ion, and therefore the $b_n \rightarrow a_n$ reaction could be expected, regardless of prior y-series history of the b-precursor. Both of the y_mb_n and y_ma_n ions are commonly observed in the peptide CID [53, 54]. However, the sequential relation of these fragments is noteworthy, especially since no similar reaction took place in the sequential CID pathway of the y_4b_4 ion (in the Figure 5 series: the expected y_4a_4 would have an *m/z* 234). Also, it

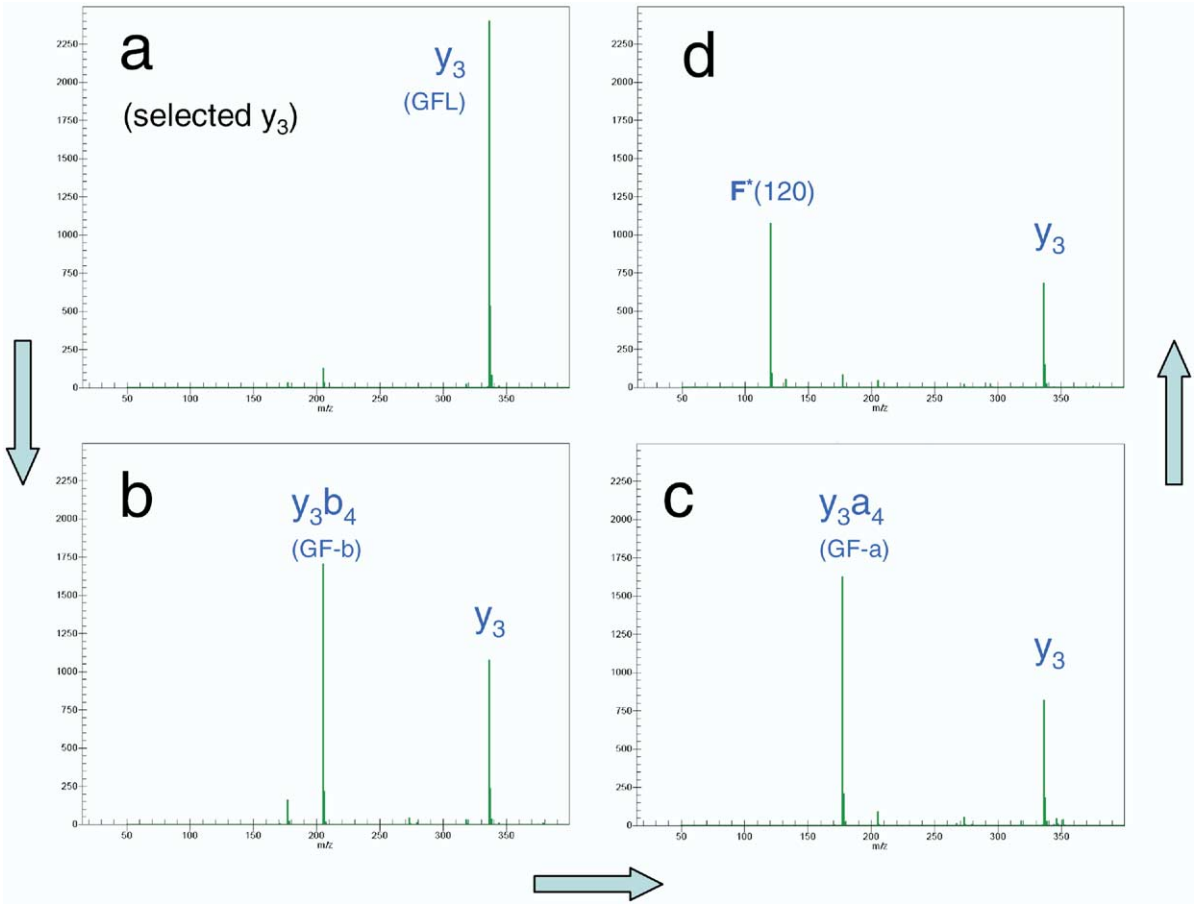

Figure 6. Multiple-resonance CID of the C-terminus fragment y_3 of YGGFL. Main RF level in H1 unchanged from the y_4 series. (**a**) Spectrum of the y_3 produced by in-source CID and isolated in AQ; (**b**) resonant excitation applied to the y_3 in CQ; (**c**) excitation applied to y_3 and y_3b_4; (**d**) excitation applied to y_3, y_3b_4, and y_3a_4.

is noteworthy that some y_2 (FL) ions were produced from y_4 (GGFL), but none from y_3 (GFL). This may suggest that the GG amino-terminal pair somehow "weakens" the G-F backbone region more than a single G does.

Next, the fragmentation of the y_2 ions was explored. The in-source CID spectrum of leucine enkephalin is shown in Figure 7a. It differed from Figure 5a because both of the AQ and CQ were operated at lower main RF amplitudes in order to shift the *m/z* transmission window towards lower mass fragments.

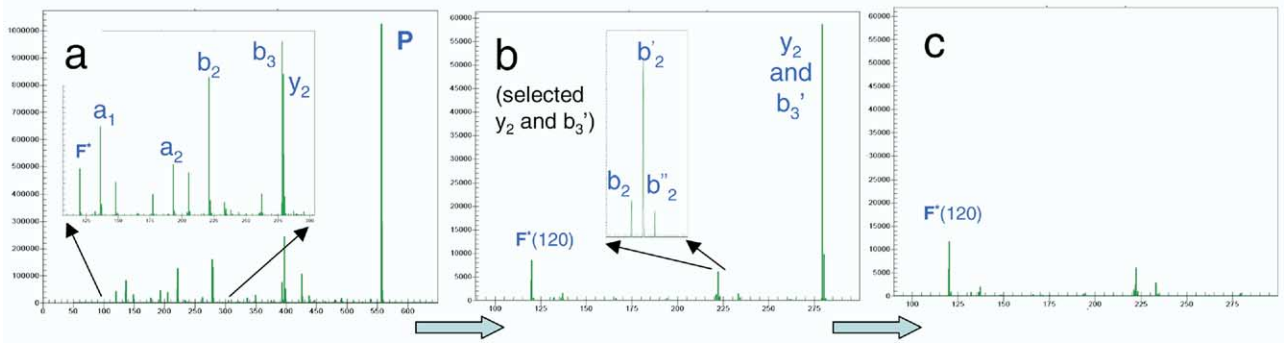

Figure 7. Multiple-resonance CID of the C-terminus fragment y_2 of YGGFL. Main RF level in H1 lowered to transmit low-mass fragments of in-source CID into AQ. (**a**) In-source CID spectrum of YGGFL; (**b**) spectrum of the *m/z*=279 doublet of y_2 the second isotope of b_3 isolated in AQ. The F* ions and the isotopic group around *m/z* 222 are produced via metastable decay in CQ of ions isolated in AQ. Isotopic pattern of peaks around *m/z* 222 indicates that they are fragments of the second isotope; (**b**) result of resonant excitation applied to the y_2: the only product is F*.

All fragments marked in the Figure 7a inset have been discussed above. The b_3 (*m/z* 278) ion has its second isotope, termed b_3' within 0.06 Da of the monoisotopic y_2 (*m/z* 279). These two ions can be resolved by the TOF mass analyzer, but not by a quadrupolar mass filter. Therefore, while the peak at 279 Da in the TOF spectrum had a clear doublet shape, we could not selectively transmit y_2 through AQ without passing b_3' with it. Thus, the ion ensemble of *m/z* ~279, selected by the RF-DC in AQ (~1 Da wide *m/z* window) shown in Figure 7b actually consisted of both y_2 and b_3'. Some of the 279 *m/z* ions selected in AQ were "hot" as a result of the intense in-source CID; they continued to dissociate in the QC even before any resonant excitation was applied as evident from Figure 7b. This metastable dissociation of some of the selected ions resulted in a formation of F* and a spectral group of three peaks around *m/z* 222 shown in the inset of Figure 8b. The *m/z* values of these peaks corresponded to the first, second and third isotope of b_2, termed b_2, b_2', and b_2'', respectively, and their relative abundance clearly indicated that they were all produced from one precursor—the second isotopic peak of b_3, the b_3'. Indeed, the most probable isotope in such a group of ions had to be the b_2', while b_2 and b_2'' had to have roughly equal probability [55, 56], in accord with experimental ratio presented by the inset in Figure 7b.

Resonant excitation of the *m/z* 279 ion led to only the increase of the F* ions' abundance suggesting it as the only fragment of y_2. By comparing the relative abundances of y_2 and b_3 from in-source CID as shown in Figure 7a, one would expect that after the mass selection step (and background decomposition of b_3'), very little of the b_3' would remain in the *m/z* 279 peak in Figure 7b. Thus, only a slight increase in intensity of the "222 group" was expected between Figure 7b and c. Additionally, some of the resonantly excited b_3' ions could have been ejected rather than dissociated. Therefore, the unchanged intensity of the "222 group" in Figure 7b and c was taken as an additional indication of their b-origin.

Branch of the N-Terminus Pathway: Complementary Formation of F and b_3 from a_4. Overall Decomposition Scheme*

All y-fragments pathways had the same final product—the immonium ion of phenylalanine, F*. This made us revisit the dissociation of a_4 – the last N-terminal fragment with phenylalanine residue. In the experiments presented in the first section of the Results addressing fragmentation of the N-terminus, the main RF amplitude was chosen to provide optimal conditions for the exclusive sequential CID in a mass range which included the leucine enkephalin parent ion (at *q*-value of ~0.25). Under these conditions the F* ions of *m/z* 120 were so far below the low-mass cutoff of the CQ that, unlike the a_1 ions with *m/z* 136, they could not be collisionally stabilized.

In the discussion on the formation of the b_3 ions, we have proposed that the reaction $a_4 \rightarrow b_3$ might have a complement $a_4 \rightarrow F^*$. In order to observe the potential production of F* from the YGGF-a (a_4) ions, we conducted two experiments at the main RF level of ~150 $V_{0\text{-}p}$ in the CQ. In the first experiment, the excitation waveform was a superposition of two sinusoids of 53 and 69 kHz, both at a 0.4 $V_{0\text{-}p}$ amplitude level, corresponding to the resonance of the *m/z* 556 (parent ion) and 425 (b_4). It was done to exclusively produce a_4 ions—the precursor for our case study. The resulting spectrum is shown in Figure 8a. In the next experiment, a 0.6 $V_{0\text{-}p}$, 74 kHz component was superimposed onto the prior excitation waveform, thus targeting the a_4 ions. The resulting CID spectrum is shown in Figure 8b. It suggested that the F* and the b_3 ions were produced in parallel from a_4. The y-axis scale was conserved between Figure 8a and b. Under the conditions of 10 mTorr of pressure in the CQ and a low-*q* (shallow potential well) we were unable to close-up the $a_4 \rightarrow F^*$ channel by lowering the amplitude of the a_4 resonant excitation. This indicated that on the millisecond time scale of excitation and detection apparent activation energies for the formation of b_3 and F* from a_4 are close.

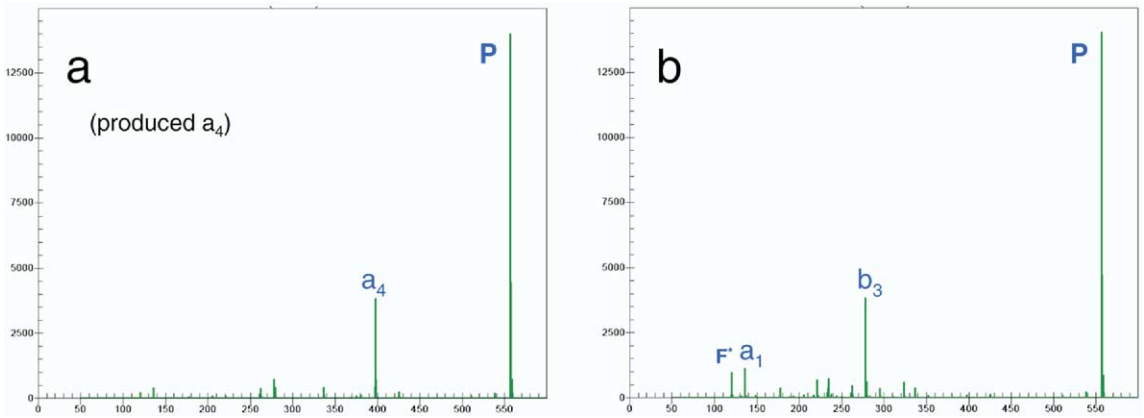

Figure 8. Multiple resonant CID of N-terminus fragment a_4 at low *q*-value in CQ. (**a**) Preparation stage: low-energy excitation applied to P and b_4 to produce a_4; (**b**) excitation applied to P, b_4, and a_4. Complementary ions b_3 and F* are produced from a_4 with roughly equal yields.

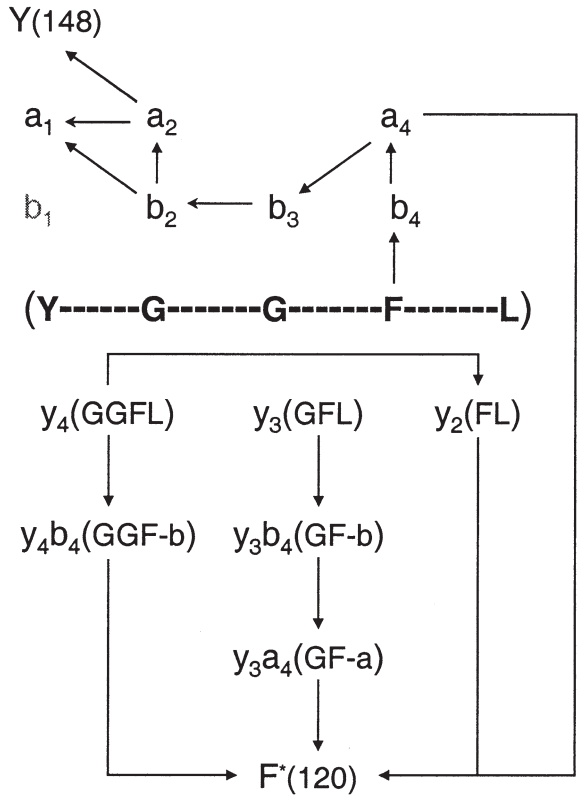

Scheme 1. The summary of the low-energy millisecond time-scale sequential decomposition pathways of leucine enkephalin and its major fragments.

Based on the pathways explored in prior sections, we were able to construct a full scheme of the low-energy sequential decomposition of leucine enkephalin and its fragments, shown in Scheme **1**. The thick arrows represent the lowest energy sequential dissociation pathway observable in the millisecond time frame. The major fragmentation pathway is $P \rightarrow b_4 \rightarrow a_4 \rightarrow b_3 \rightarrow b_2$, which was realized without any significant branching, except for some possible competition between the formation of b_3 and F* from a_4. For reasons discussed above, under the experimental conditions described, the last two stages of decomposition were not exclusive. The b_2 fragmented into a_2 and a_1 simultaneously. Similarly, a_2 fragmented simultaneously into a_1 and into the *m/z* 148 ion. It is unclear whether these channels occur in parallel or proceed in sequence with a high rate caused by overheating of the respective precursors.

In order to dissociate into the y-ions, leucine enkephalin had to be excited more intensely than for $P \rightarrow b_4$, and in this sense, reactions leading to the formation of y-ions from P were not the lowest-activation channels. Thus, the y-fragments are included into the scheme but not connected with the parent ion by arrows. In the described instrumental setup, it was simpler to employ alternative activation protocols such as axial in-quadrupole or axial in-source CID, to produce the first generation of y-fragments. The latter were isolated and subjected to a well-controlled soft resonant excitation. Their CID was exclusive and sequential, hence these channels are marked with solid arrows completing the diagram of low-energy millisecond time scale gas-phase decomposition pathways of leucine enkephalin.

Summary and Future Research

The instrumentation setup and operation mode of the multiple-resonance excitation CID method applied to a continuous ion beam in the collision-cell quadrupole of an instrument with a TOF MS analyzer has been presented. A qualitative comparison between the spectral patterns of an axial acceleration versus single-resonance radial CID of the leucine-enkephalin model peptide was performed under the same conditions in the collision cell. The analysis of relative intensities of the most common fragments of resonant CID revealed complexity of the actual fragmentation mechanisms due to the likely simultaneous activation of direct and sequential fragmentation channels. Dependence of the relative intensities of fragments on the excitation amplitude of single resonance strongly suggested that sequential fragmentation did occur, in contrast with the commonly accepted concept of the soft, target-specific mode of the energy deposition in resonant CID.

As a preamble for a detailed study of the actual CID mechanisms of leucine enkephalin, it is necessary to first establish pathways of sequential decomposition which involve its major fragments. The multiple-resonance low-energy CID experiments allowed identification of the origins and products of all of the major fragments of leucine enkephalin. The presented experimental results were combined into one diagram, which describes the lowest-energy sequential decomposition pathways of these agents, observable on a millisecond excitation time-scale. While most of the reactions observed for the N-terminus fragments were witnessed in the past, several are new, to the best of our knowledge. Observation of a rearrangement resulting from the internal amino acid loss from the a_4 fragment has been observed in trap-MS instruments in the past, but not in the continuous beam experiments. Also, the neutral loss of 45 Da from a_2 and y_4b_4 appears intriguing and its mechanism(s) will be addressed in our future research. As a general trend, the counterpart of dissociation with tyrosine always retained the charge. The C-terminus fragmentation involved separate pathways for y_4, y_3, and y_2 ions with one cross-over from y_4 into y_2. In all C-terminus pathways, the dissociation counterpart with phenylalanine retained the charge, and overall, formation of the internal b-ions from y-ions prevailed (again, except for the minor $y_4 \rightarrow y_2$ channel, and $y_2 \rightarrow F^*$). The a_4 ion, which had tyrosine on the N-terminus and phenylalanine on the C-terminus, presented a special case. In its dissociation, the complementary b_3 (with the charge retained on the counterpart with tyrosine) and F* (the charge on the phenylalanine) ions were observed, simultaneously.

One could argue that sequential low-energy decomposition realizes reactions which may not necessarily be followed in the course of dissociation of a moderately excited leucine enkephalin itself. Indeed, sequential product ions were treated as "new parents" for the next generation of CID, as if the whole history of their formation was irrelevant. This is not the case in real CID experiments, where the extensive fragmentation is observed as a result of over-excitation of the leucine enkephalin itself, rather than being caused by a direct soft activation of primary, secondary, etc. fragments. The sequential dissociation patterns do, however, assist in the interpretation of complex CID cases involving multi-channel parallel dissociation and formation of complementary ions, which is the subject of our current research. Moreover, a delicate sequential fragmentation with opening single-channel pathways can be advantageous in a variety of studies targeting structural identification. For example, it can be used in phospho-peptide investigations, where several steps of dissociation can realize MS^n studies in order to identify the phosphorylation sites. This particular application of the presented method is also currently under investigation.

Instrumentally, these studies were made possible because of the ability of the instrument to conduct three modes of CID, in-source, in the axial-acceleration fashion in the collision cell, and/or by means of the multiple-frequency resonance in the collision cell. Fragment ion populations were analyzed by a TOF MS with the resolving power and mass measurement accuracy greatly exceeding those of the triple quadrupoles or ion traps. To some extent, the presented instrumental arrangement combined functional features of a triple quadrupole with those of a 3-D ion trap and a Q-TOF. This study was conducted using an interactive user interface for the multiple-resonance waveform generation, but the simplicity of the method allows a straightforward automation of any of the experimental series presented. Taking into account a millisecond time scale of excitation in the presented experiments, several stages of an automated data-dependent MS^n experiment could be realized in a low sub-second time frame, if so desired.

Acknowledgments

The authors gratefully acknowledge collaboration with Drs. L. Cousins and R. Javahery in instrument development, Dr. J. Laskin and Professor G. Glish for fruitful discussions on parts of the presented material.

References

1. Gauthier, J. W.; Trautman, T. R.; Jacobson, D. B. Sustained off-resonance irradiation for collision-activated dissociation involving Fourier transform mass spectrometry. Collision-activated dissociation technique that emulates infrared multiphoton dissociation. *Anal. Chim. Acta* **1991,** *246*, 211.
2. Katriczky, A. R.; Watson, C. H.; Dega-Szafran, Z.; Eyler, J. R. Collisionally Activated Dissociation of Some Pyridinium Cations: Novel Fragmentation Pathways. *Org. Mass Spectrom.* **1989,** *24*, 1017–1021.
3. Dunbar, R. C.; Zaniewski, R. C. Infrared Multiphoton Dissociation of Styrene Ions by Low-Power Continuous CO2 Laser Irradiation. *J. Chem. Phys.* **1992,** *96*, 5069–5075.
4. Freitas, M. A.; Hendrickson, C. L.; Marshall, A. G. Gas Phase Activation Energy for Unimolecular Dissociation of Biomolecular Ions Determined by Focused Radiation for Gaseous Multiphoton Energy Transfer (FRAGMENT). *Rapid Commun. Mass Spectrom.* **1999,** *13*, 1639–1642.
5. Dunbar, R. C.; McMahon, T. B.; Thoelmann, D.; Tonner, D. S.; Salahub, D. R.; Wei, D. Zero-Pressure Thermal-Radiation-Induced Dissociation of Gas-Phase Cluster Ions: Comparison of Theory and Experiment for (H2O)2Cl- and (H2O)3Cl-. *J. Am. Chem. Soc.* **1995,** *117*, 12819–12825.
6. Laskin, J.; Futrell, J. H. Collisional Activation of Peptide Ions in FT-ICR Mass Spectrometry. *Mass Spectrom. Rev.* **2003,** *22*, 158–181.
7. Schnier, P. D.; Jurchen, J. C.; Williams, E. R. The Effective Temperature of Peptide Ions Dissociated by Sustained Off-Resonance Irradiation Collisional Activation in Fourier Transform Mass Spectrometry. *J. Phys. Chem. B* **1999,** *103*, 737–745.
8. Cole, R. B.; LeMeillour, S.; Tabet, J. C. Surface-Induced Dissociation of Protonated Peptides: Implications of Initial Kinetic Energy Spread. *Anal. Chem.* **1992,** *64*, 365–371.
9. Asano, K. G.; Goeringer, D. E.; McLuckey, S. A. Thermal Dissociation in the Quadrupole Ion Trap: Ions Derived from Leucine Enkephalin. *Int. J. Mass Spectrom.* **1999**, *185/187*, 207–219.
10. Vékey, K.; Somogyi, Á.; Wysocki, V. H. Average Activation Energies of Low-Energy Fragmentation Processes of Protonated Peptides Determined by a New Approach. *Rapid Commun. Mass Spectrom.* **1998,** *10*, 911–918.
11. Alexander, A. J.; Boyd, R. K. Experimental Investigations of Factors Controlling the Collision Induced Dissociation Spectra of Peptide Ions in a Tandem Hybrid Mass Spectrometer. I. Leucine Enkephalin. *Int. J. Mass Spectrom. Ion Processes* **1989,** *90*, 211–240.
12. Heeren, R. M. A.; Vékey, K. A Novel Method to Determine Collisional Energy Transfer Efficiency by Fourier Transform Ion Cyclotron Resonance Mass Spectrometry. *Rapid Commun. Mass Spectrom.* **1998,** *12*, 1175–1181.
13. Lim, H.; Schultz, D. O.; Yu, C.; Hanley, L. Relative Dissociation Energies of Protonated Peptides by Electrospray Ionization/Surface-Induced Dissociation. *Anal. Chem.* **1999,** *71*, 2307–2317.
14. Mohammed, S.; Chalmers, M. J.; Gielbert, J.; Ferro, M.; Gora, L.; Smith, D. C.; Gaskell, S. J. A Novel Tandem Quadrupole Mass Spectrometer Allowing Gaseous Collisional Activation and Surface Induced Dissociation. *J. Mass Spectrom.* **2001,** *36*, 1260–1268.
15. Nikolaev, E. N.; Somogyi, A.; Smith, D. L.; Gu, C.; Wysocki, V. H.; Martin, C. D.; Samuelson, G. L. Implementation of Low-Energy Surface-Induced Dissociation (eV SID) and High-Energy Collision-Induced Dissociation (keV CID) in a Linear Sector-TOF Hybrid Tandem Mass Spectrometer. *Int. J. Mass Spectrom.* **2001,** *212*, 535–551.
16. Guo, X.; Duursma, M. C.; Al-Khalili, A.; Heeren, R. M. A. Experimental Calibration of the SORI-CID Internal Energy Scale: Energy Uptake and Loss. *Int. J. Mass Spectrom.* **2003,** *225*, 71–82.
17. Vachet, R. W.; Glish, G. L. New Method to Study the Effects of Peptide Sequence on the Dissociation Energetics of Peptide Ions. *J. Am. Soc. Mass Spectrom.* **1998,** *9*, 175–177.

18. Vachet, R. W.; Ray, K. L.; Glish, G. L. Origin of Product Ions in the MS/MS Spectra of Peptides in a Quadrupole Ion Trap. *J. Am. Soc. Mass Spectrom.* **1998,** *9*, 341–344.
19. Dongre, A. R.; Jones, J. L.; Somogyi, A.; Wysocki, V. H. Influence of Peptide Compsition, Gas-Phase Basicity, and Chemical Modification on Fragmentation Efficiency: Evidence for the Mobile Proton Model. *J. Am. Chem. Soc.* **1996,** *118*, 8365–8374.
20. Harrison, A. G.; Yalcin, T. Proton Mobility in Protonated Amino Acids and Peptides. *Int. J. Mass Spectrom. Ion Processes* **1997**, *165/166*, 339–347.
21. Csonka, I. P.; Paizs, B.; Lendvay, G.; Suhai, S. Proton Mobility in Protonated Peptides: A Joint Molecular Orbital and RRKM Study. *Rapid Commun. Mass Spectrom.* **2000,** *14*, 417–431.
22. Nold, M. J.; Cerda, B. A.; Wesdemiotis, C. Proton Affinities of the N- and C-Terminal Segments Arising Upon the Dissociation of the Amide Bond in Protonated Peptides. *J. Am. Soc. Mass Spectrom.* **1999,** *10*, 1–8.
23. Paizs, B.; Suhai, S. Towards Understanding Some Ion Intensity Relationships for the Tandem Mass Spectra of Protonated Peptides. *Rapid Commun. Mass Spectrom.* **2002,** *16*, 1699–1702.
24. Paizs, B.; Suhai, S.; Harrison, A. G. Experimental and Theoretical Investigation of the Main Fragmentation Pathways of Protonated H-Gly-Gly-Sar-OH and H-Gly-Sar-Sar-OH. *J. Am. Soc. Mass Spectrom.* **2003,** *14*, 1454–1469.
25. Paizs, B.; Suhai, S. Towards Understanding the Tandem Mass Spectra of Protonated Oligopeptides. 1: Mechanism of Amide Bond Cleavage. *J. Am. Soc. Mass Spectrom.* **2004,** *15*, 103–113.
26. Morgan, D. G.; Bursey, M. M. A Linear Free-Energy Correlation in the Low-Energy Tandem Mass Spectra of Protonated Tripeptides Gly-Gly-Xxx. *Org. Mass Spectrom.* **1994,** *29*, 354–359.
27. Polce, M. J.; Ren, D.; Wesdemiotis, C. Dissociation of the Peptide Bond in Protonated Peptides. *J. Mass Spectrom.* **2000,** *35*, 1391–1398.
28. Whitehouse, C.M.; Rakov, V.S.; Borisov, O.V.; Welkie, D.; Tomski, I.; Javahery, G.; Cousins, L. Multiple Quadurpole 2D Trap TOF Mass Spectrometer. *Proceedings of the 51st ASMS Conference on Mass Spectrometry and Allied Topics*; Montreal, Quebec, Canada, June, 2003; on CD-ROM, AO31856.pdf.
29. Rakov, V. S.; Whitehouse, C. M. Excitation of Ions by High-Harmonic Frequency Components in Paul and Pening Traps and Ion Guides. I. Selective Simultaneous Excitation of High Charge States with Clipped Sinusoidal and Nonharmonic Waveforms in Linear Quadrupole Ion Guide. *Eur. J. Mass Spectrom*. **2004,** *10*, 173–186.
30. Huddleston, M. J.; Annan, R. S.; Bean, M. F.; Carr, S. A. Selective Detection of Phosphopeptides in Complex Mixtures by Electrospray Liquid Chromatography/Mass Spectrometry. *J. Am. Soc. Mass Spectrom.* **1993,** *4*, 710–717.
31. Schneider, B. B.; Douglas, D. J.; Chen, D. D. Y. Collision-Induced Dissociation of Bradykinin ions in the Interface Region of an ESI-MS. *J. Am. Soc. Mass Spectrom.* **2001,** *12*, 772–779.
32. Analytica of Branford, I. Corsair MS and Aviator Software Manual. 2003; http://www.aob.com.
33. Carrico, J. P. Applications of inhomogeneous oscillatory electric field in ion physics. *Dyn. Mass Spectrom.* **1972,** *3*, 1.
34. Dehmelt, H. G. Radio-frequency spectroscopy of stored ions. I. Storage. *Advan. At. Mol. Phys.* **1967,** *3*, 53.
35. Major, F. G.; Dehmelt, H. G. Exchange-collision technique for the rf (radio-frequency) spectroscopy of stored ions. *Phys. Rev.* **1968,** *170*, 91.
36. Slater, J. C.; Frank, N. H. *Introduction to Theoretical Physics*, Chap IV; McGraw-Hill: New York and London, 1933.
37. Landau, L. D.; Lifshitz, E. M. *Theoretical Physics*, Vol. I, Chap V, Section 26; Pergamon: Oxford, 1969.
38. Resnick, R.; Holliday, D. *Physics for Students of Science and Engineering*, Part I, Chap XV, Section 9; John Wiley and Sons, Inc.: New York and London, 1954.
39. Wuerker, R. F.; Shelton, H.; Langmuir, R. V. Electrodynamic containment of charged particles. *J. Appl. Phys.* **1959,** *30*, 342.
40. Todd, J. F. J.; Lawson, G.; Bonner, R. F. In *Quadrupole Mass Spectrometry and Its Applications*; Peter H, D., Ed.; AIP Press: Woodbury, NY, 1995; Chapter VIII.
41. Belov, M. E.; Nikolaev, E. N.; Harkewicz, R.; Masselon, C. D.; Alving, K.; Smith, R. D. Ion Discrimination During Ion Accumulation in a Quadrupole Interface External to a Fourier Transform Ion Cyclotron Resonance Mass Spectrometer. *Int. J. Mass Spectrom.* **2001,** *208*, 205–225.
42. Collings, B. A.; Stott, W. R.; Londry, F. A. Resonant Excitation in a Low-Pressure Linear Ion Trap. *J. Am. Soc. Mass Spectrom.* **2003,** *14*, 622–634.
43. Whitehouse, C. M.; Dresch, T.; Andrien, B. U.S.A. Patent, **2000**, 6,011,259.
44. Cousins, L. M.; Thomson, B. A. MS3 Using the Collision Cell of a Tandem Mass Spectrometer System. *Rapid Commun. Mass Spectrom.* **2002,** *16*, 1023–1034.
45. Roepstroff, P.; Fohlman, J. Proposal for a common nomenclature for sequence ions in mass spectrometry of peptides. *J. Biomed. Mass Spectrom.* **1984,** *11*, 601.
46. Biemann, K.; Scoble, H. A. Characterization by Tandem Mass Spectrometry of Structural Modifications in Proteins. *Science* **1987,** *237*, 992–998.
47. Johnson, R. S.; Martin, S. A.; Biemann, K. Collision-Induced Fragmentation of (M + H)+ Ions of Peptides. Side Chain Specific Sequence Ions. *Int. J. Mass Spectrom. Ion Processes* **1988,** *86*, 137–154.
48. Laskin, J.; Futrell, J. Entropy is the Major Driving Force for Fragmentation of Proteins and Protein-Ligand Complexes. *J. Phys. Chem. A* **2003,** *107*, 5836.
49. Vachet, R. W.; Bishop, B. M.; Erickson, B. W.; Glish, G. L. Novel Peptide Dissociation: Gas-Phase Intramolecular Rearrangement of Internal Acid Residues. *J. Am. Chem. Soc.* **1997,** *119*, 5481–5488.
50. Ambihapathy, K.; Yalcin, T.; Leung, H.-W.; Harrison, A. G. Pathways to Immonium Ions in the Fragmentation of Protonated Peptides. *J. Mass. Spectrom*. **1997,** *32*, 209–215.
51. Yalcin, T.; Khouw, C.; Csizmadia, I. G.; Peterson, M. R.; Harrison, A. G. Why are B Ions Stable Species in Peptide Spectra? *J. Am. Soc. Mass Spectrom.* **1995,** *6*, 1165–1174.
52. Nold, M. J.; Wesdemiotis, C.; Yalcin, T.; Harrison, A. G. Amide Bond Dissociation in Protonated Peptides. Structures of the N-Terminal Ionic and Neutral Fragments. *Int. J. Mass Spectrom. Ion Processes* **1997,** *164*, 137–153.
53. Falick, A. M.; Hines, W. M.; Medzihradszky, K. F.; Baldwin, M. A.; Gibson, B. W. Low-Mass Ions Produced from Peptides by High-Energy Collision-Induced Dissociation in Tandem Mass Spectrometry. *J. Am. Soc. Mass Spectrom.* **1993,** *4*, 882–893.
54. Medzihradszky, K. F.; Hall, S. C.; Maltby, D. A.; Hines, W. M.; Burlingame, A. L. *Techniques in Protein Chemistry,* II; Academic: San Diego, 1991.
55. Rockwood, A. L.; Kushnir, M. M.; Nelson, G. J. Dissociation of Individual Isotopic Peaks: Predicting Isotopic Distributions of Product Ions in MSn. *J. Am. Soc. Mass Spectrom.* **2003,** *14*, 311–322.
56. Borisov, O.V.; Rakov, V.S.; Welkie, D.; Javahery, G.; Cousins, L.; Wihiteouse, C.M. Evaluating Performance of a Bew Multiple Ion Guide 2D Trap TOF inMS and MS2, MS3 Acquisition Modes for Proteomics and Analysis of Small Molecules. *Proceedings of the 51st ASMS Conference on Mass Spectrometry and Allied Topics*; Montreal, Quebec, Canada, June, 2003; on CD-ROM, AO32096.Pdf.